



Hall, W., Rico-Ramirez, M., & Stefan, K. (2015). Classification and Correction of the Bright Band using an operational C-band Polarimetric Radar. *Journal of Hydrology*, 531(2), 248-258. DOI: 10.1016/j.jhydrol.2015.06.011

Peer reviewed version

Link to published version (if available):
[10.1016/j.jhydrol.2015.06.011](https://doi.org/10.1016/j.jhydrol.2015.06.011)

[Link to publication record in Explore Bristol Research](#)
PDF-document

University of Bristol - Explore Bristol Research

General rights

This document is made available in accordance with publisher policies. Please cite only the published version using the reference above. Full terms of use are available:
<http://www.bristol.ac.uk/pure/about/ebr-terms.html>

Classification and Correction of the Bright Band using an operational C-band Polarimetric Radar

WILL HALL and MIGUEL ANGEL RICO-RAMIREZ

Department of Civil Engineering, University of Bristol, Bristol, UK

STEFAN KRÄMER

Institute for Technical and Scientific Hydrology Ltd., Engelbosteler Damm 22, D-30167 Hanover, Germany

Corresponding Author's Contact Information:

Phone: (+44) 07521277178

Email: w.hall@bristol.ac.uk

ABSTRACT

The Bright Band (BB) is a region of enhanced reflectivity in weather radar scans associated with frozen hydrometeors forming a liquid coating as they fall through the melting layer. This enhancement can cause the radar to overestimate precipitation quantities at the surface. The main objective of this study is to develop a hydrometeor classification algorithm that can use dual-polarisation measurements as the only input to classify the BB area. An effort has been made to replicate the current UK Met Office operational method for BB classification. This involves the use of Numerical Weather Prediction outputs of freezing level heights with an assumption of a constant BB thickness. Vertical Profiles of Reflectivity (VPR) can then be used to correct for the reflectivity enhancement. A mean apparent VPR computed from reflectivity measurements at multiple elevation angles is compared to two idealised VPR methods. For validation the corrected 1.5° elevation scans are compared to surface rain gauge observations and lower elevation scans over the course of 7 events. The hydrometeor classification methods showed the greatest error reductions, with the freezing level forecast method performing well when the BB thickness was within 700 m, but poorly when there was more variation. Overall the idealised VPRs allowed for the greatest BB corrections in comparison to the mean profile.

1. Introduction

Quantitative estimation of precipitation by weather radars is affected by many sources of error, as described in reviews by *Joss and Waldvogel* (1990) and *Villarini and Krajewski* (2009). A significant error source is through uncertainties caused by variation in the vertical profile of reflectivity (VPR). This can be due to orographic enhancement, evaporation below the beam, and particularly the Bright Band (BB); which was observed at an early stage by *Austin and Bemis* (1950) and *Atlas and Banks* (1950). The BB is located in a region, several hundred meters deep, below the 0°C isotherm in which falling snow flakes or graupel will gradually melt and form a liquid coating which will give the appearance of intense rain in reflectivity scans. An in-depth study by *Fabry and Zawadzki* (1995) revealed the nonsphericity of melting hydrometeors and density effects are additional important causes of the reflectivity enhancement. Overall this will cause overestimation of rainfall by a factor of 2-5 (*Joss and Waldvogel* 1990), and could lead to false alarms of flood events. Additionally, snow above the melting layer can cause reductions by 1 to 2 dB in comparison to rain below (*Fabry and Zawadzki* 1995).

The current UK Met Office operational algorithm to identify the freezing level height, and so the BB region, is described by *Kitchen et al* (1994) and *Harrison et al* (2000). The Met Office Unified Mesoscale Model is used to forecast the freezing level height with an RMSE of 150m (*Mittermaier and Illingworth* 2003) which is within the 200m error range suggested by *Kitchen et al.* (1994). *Sanchez-Diezma et al.* (2000) proposed a method for BB identification that input averaged VPRs from volumetric scans of previous BB events to create simulated VPRs. They concluded that with enough elevations, and an efficient scanning strategy, identification was possible within 70 km of the radar. Beyond that distance the amount of elevations intersecting the radar decreased and beam spreading caused too great a loss in resolution. Alternately, the BB region can be determined through hydrometeor classification directly from dual-polarisation radar measurements (*Herzogh and Jameson* 1992; *Straka et al* 2000; *Liu and Chandrasekar* 2000) or from Range Height Indicator (RHI) polarimetric observations (*Schusse et al* 2011). These measurements contain information on the size, shape, and spatial orientation of hydrometeors (*Bringi and Chandrasekar* 2001). A distinct minimum in the cross correlation coefficient (ρ_{hv}) (*Matrosov et al.* 2007; *Park et al.* 2009; *Qi et al.* 2013) and maximum in the differential reflectivity (Z_{dr}) are found to be coincident with the 1° isotherm (*Aydin et al* 1984; *Ryzhkov and Zrnica* 1998). The linear depolarisation ratio (LDR) also has a very distinct signal in melting snow (*Caylor et al.* 1990; *Rico-Ramirez et al.* 2005). Some of the methods to classify melting snow include fuzzy logic systems (*Rico-Ramirez et al.* 2005), neural networks or decision tree methods (*Liu and Chandrasekar* 2000).

There are several approaches for the correction of VPR variation. A widely used method involves the creation of an apparent VPR formed from azimuthally averaged scans (*Koistinen* 1991; *Matrosov et al* 2007; *Zhang et al* 2008). Preferably multiple elevations or volumetric scans would be used, with only the initial 40 km being averaged (*Andrieu and Creutin* 1995). *Zhang and Qi* (2010) suggest a different approach in which the BB area is determined from radar reflectivity distributions and all ranges within this BB area are averaged. *Kitchen et al* (1994) created a parameterised profile that includes low-level orographic growth, the BB, and reduction in reflectivity due to snow. This method assumes a fixed 700m BB thickness and applies the reflectivity reduction to pixels within the scan individually. *Kitchen* (1997) refined the previous method implementing a dual layer exponential decay profile above the melting layer to improve upon the original usage of a climatological profile. The decay profile is split due to accelerated aggregation of snow particles above the -6°C layer (*Fabry and Zawadzki* 1995). *Tabary et al* (2007) use a similar idealised profile formed from 4 parameters that can take a limited number of values based upon climatology. *Rico-Ramirez et al* (2005) built equations to form idealised profiles from a substantial amount of S-band radar data. *Vignal et al* (2000) compare three methods to correct for VPR uncertainty in complex terrain in Switzerland. A climatological profile, formed from several years of data, significantly improved the accuracy of the rainfall estimations, and a mean VPR formed over a radius of 70km improved the accuracy further. For the third approach localised apparent VPRs over areas of 20km by 20km were created, although this method was more computationally intensive and less robust, so it was suggested the mean profile is optimal for operational usage. *Kirstetter et al* (2013) implement a novel VPR identification technique, in similarly difficult terrain, with good results by using physically based constraints and continually updating VPR characteristics. *Delrieu et al.* (2009) implement algorithms by *Steiner et al.* (1995) and *Sanchez-Diezma et al.* (2000) to initially separate rain events into stratiform and convective, before applying BB corrections methods. They find an inversion VPR technique, initially proposed by *Andrieu and Creutin* (1995), results in a more positive impact upon bias reduction when compared to an apparent normalised VPR. *Illingworth and Thompson* (2012) propose the use of LDR for BB correction after finding correlations between LDR and difference in Z between the BB peak and the rain below. *Hazenberg et al* (2013) compare the correctional abilities of VPRs estimated using Eulerian compared to a new Lagrangian implementation. They also present an approach to identify the impact of uncertainty within the VPRs on rainfall estimation.

The majority of previous research has used S- or X- band measurements whereas the UK operational radar network consists predominantly of C-band radars. At C-band wavelengths the detection of wet aggregates could be enhanced in comparison to S- band due to a greater contrast in LDR, Z_{dr} and ρ_{hv} (Zrníc and Ryzhkov 1999). This paper assesses the ability of two different BB classification and removal methods that will use hydrometeor classification and BB correction using idealised and averaged VPRs. The benefit of these methods is the lack of reliance upon surface observations and computationally expensive forecasts and instead the utilisation of data only from operational polarimetric radars. Section 2 presents characteristics of the radar and rain gauge data sets. Section 3 explains the two BB classification methods that will be compared. Section 4 describes the four different BB correction methods using mean and idealised reflectivity profiles. Section 5 addresses the radar and rain gauge validation comparisons. Conclusions and summary of the work are presented in section 6.

2. Data Processing and Method

Scans from an operational C-band polarimetric radar located in Chenies, UK, have been analysed. This radar has been recently upgraded to dual-polarisation by the UK Met Office. The radar makes multiple dual-polarisation measurements, including ρ_{hv} , Z_{DR} , and LDR. The scanning strategy for the Chenies radar includes 5 PPI scans with long pulse (600 ms) measurements, of which only the lowest two, at 0.5° and 1.4° , include LDR measurements. The lower scan at 0.5° suffers greatly from ground clutter and beam blockage. There are also 6 short pulse scans (300 ms) which are utilised when forming an average VPR. Range bin lengths are 600 m with a total range of 255 km and a radar beam width of 1° .

A total of 14 rainfall events from between December 2013 and June 2014 were used. The events were selected as having suitable characteristics due to the appearance of annular regions of enhanced reflectivity, enhanced LDR, decreased ρ_{hv} , and increased Z_{dr} , as in Figure 1. Each event lasts on average for over 2 hours, and contains at least 20 scans each. Four methods for classification and correction of the BB will be used, which will be detailed in the following subsections. An initial study documented in *Hall et al (2014)* provides the initial research for this project into melting layer classification.

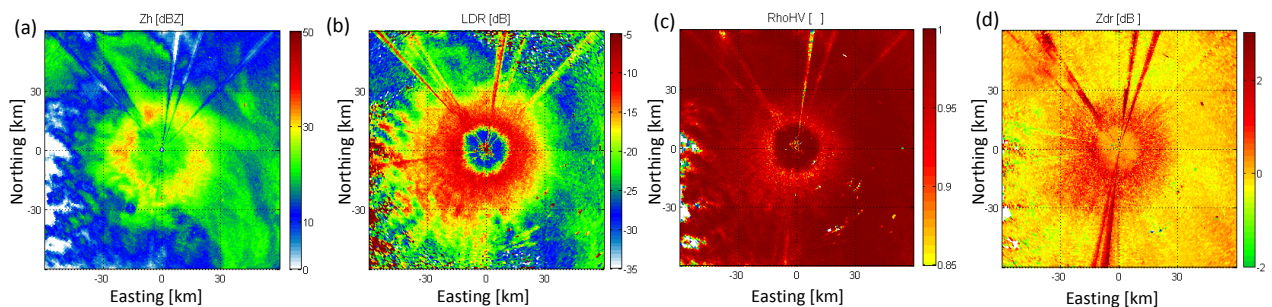


FIG. 1. Example of an observed BB on 12/02/2014 from measurements of Z_h (a), LDR (b), ρ_{hv} (c), and Z_{DR} (d).

The Environment Agency (EA) provided 12 gauges located within 250km of the radar site in Chenies, and the Met Office provided 50 gauges as part of the Met Office Integrated Data Archive System (MIDAS) that are located in the same region. The 62 gauges are shown on the map in Figure 2. The MIDAS gauges have hourly time steps with measurements from tipping bucket type gauges. The EA gauges have recordings every 15 minutes and are tipping bucket gauges. Rain gauge data sets were manually checked to remove gauges that repeatedly produced unrealistic values. The EA gauge data was already quality controlled with the data quality labelled. *Habib et al (2001)* and *Ciach (2003)* investigated errors in multiple co-located tipping bucket rain gauge measurements, finding relative standard errors of between 2.3% and 2.9% for moderate rainfall intensity at a 15 min timescale. Rain gauge sampling errors occurred during very light as well as intense rainfall due to the tipping sampling mechanism, though when time scales of more than 15 minutes were used these decreased greatly. To make an allowance for this the EA gauges will be accumulated hourly, as only scattered single gauges are available which makes more in depth analysis difficult. Attenuation can be a major contribution to radar error, and enhanced by radome wetting (*Steiner et al 1999*), however it has been checked by analysing the differential phase shift (Φ_{DP}) for each of the events used. Within the BB regions Φ_{DP} remained below 10° , though this could still cause minor underestimation of rainfall quantities.

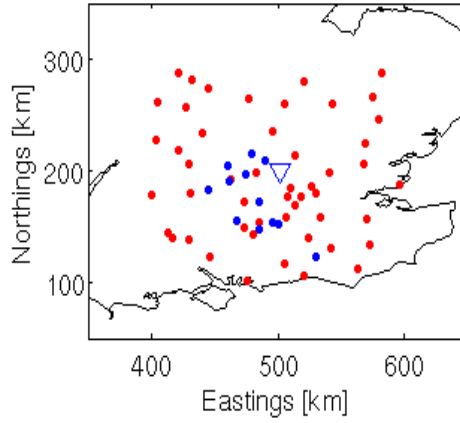


FIG. 2. MIDAS (red) and EA (blue) rain gauge locations (dots), with the all gauges falling within the 250 km radius of the radar (blue triangle).

In order to evaluate and compare the BB classification and correction methods, that will be described in detail in the subsequent sections, the following statistical metrics will be used,

Mean Absolute Error:

$$MAE = \frac{1}{n} \sum_{k=1}^n (r_k - g_k) \quad (1)$$

Root Mean Square Error:

$$RMSE = \sqrt{\frac{1}{n} \sum_{k=1}^n (r_k - g_k)^2} \quad (2)$$

Relative Mean Bias:

$$RMB = \frac{\frac{1}{n} \sum_{k=1}^n (r_k - g_k)}{\bar{G}} \quad (3)$$

where n is the number of gauge-radar observation pairs, r_k is the radar estimated rainfall at gauge location k , and g_k is the co-located rain gauge measurement. \bar{G} is the mean of the rain gauge measurements for that hour.

3. Classification of Bright Band Region

It is difficult to classify precipitation based on strict boundaries from polarimetric variables because hydrometeor observation sets are not mutually exclusive (*Doviak and Zrnica 1993; Liu and Chandrasekar 2000; Park et al 2009*). Fuzzy logic is a method that provides an alternative to Boolean logic type methods (*Straka and Zrnica 1993*) for hydrometeor classification due to the ability to handle uncertainty naturally (*Mendel 1995; Vivekanandan et al 1999*). The selected events were split into a group of 7 for validation purposes and 7 for a calibration database of values to make up the membership functions. Clutter was removed using an algorithm demonstrated in *Rico-Ramirez and Cluckie (2008)* which utilises fuzzy and Bayes classifiers trained using C-band dual-polarisation measurements.

Regions of rain, snow and melting snow were manually classified with reference to the dual-polarisation measurements, enhanced reflectivity, and knowledge of the freezing level from model reanalysis temperature

profiles. Vertical profiles of various polarimetric measurements were formed by *Brandes and Ikeda (2004)* which aided in classification. From the 7 calibration database events more than 180,000 data points were selected that were safely within these regions. Without direct, in situ measurements in the vertical of drop size distribution and air temperatures it is difficult to precisely classify the different hydrometeor regions. However with the large database size and knowledge from previous research this method for hydrometeor classification is generally proven to be robust. Data points were selected with a program which allowed the user to highlight individual pixels and output their associated values into a separate file. The values associated with the four measurements (Z_h , Z_{DR} , LDR, and ρ_{hv}) are then formed into Membership Functions (MFs) as shown in Figure 3. Initially, three probability density functions were used to cover rain, snow and melting snow however as the focus was solely on the melting snow classification it proved to be more robust to use only two MFs; one for melting snow and one for a rain and snow mixture.

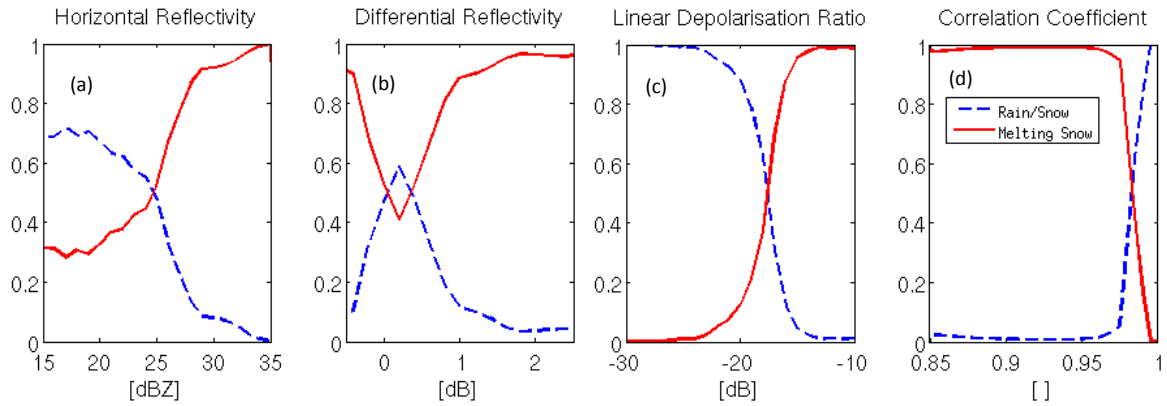


FIG. 3. Membership functions for Z_h (a), Z_{DR} (b), LDR (c), and ρ_{hv} (d) to classify hydrometeors.

At all points the MFs are non-zero so that the product of all four MFs cannot be nullified. A fuzzy logic system, explained in detail by *Mendel (1995)* is used to map measurements of the four variables into hydrometeor types. The BB region begins when moving outwards from the centre along an azimuth an average of 4 in 5 are pixels classified as melting snow and ends when this average drops below 4. This average makes an allowance for noise or incorrectly identified pixels. A moving average filter is applied, which assigns lower weight to outliers, to the top and bottom boundaries of the BB area to smooth inconsistencies. Pixels that contain anomalous values or erroneous data are set as ‘undefined’.

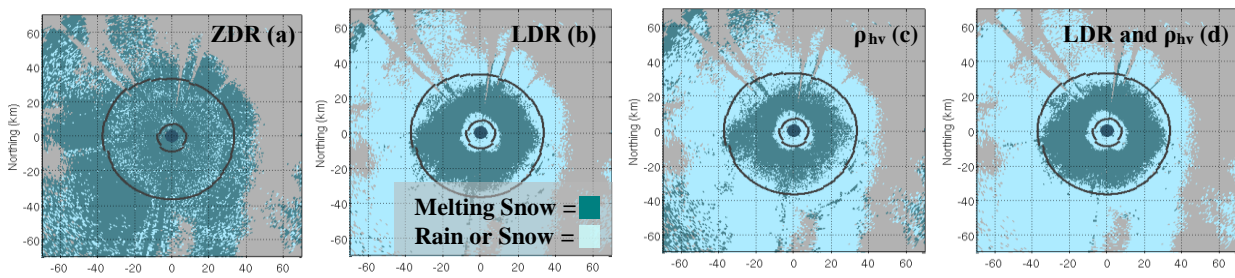


FIG. 4. Hydrometeor classification using Z_{DR} (a), LDR (b), ρ_{hv} (c), and LDR and ρ_{hv} (d), in which dark blue represents melting snow, and the rain/snow mixture as light blue. Black rings indicate the freezing level output from reanalysis data with the inner ring indicating 700m below the freezing level.

The hydrometeor classifier has been tested against 110 validation scans from 7 events in which over 200,000 pixels were originally classified into melting snow or ‘Rain/Snow’. Many radar sites do not measure LDR due to the inability to measure other polarimetric variables simultaneously; so the classifier was tested using different combinations of variables. Figure 4 shows the hydrometeor classification results using each measurement, overlaid with the freezing level output from reanalysis data, which will be explained further in section 3.1. Results from *Zrnich et al (2001)* showed that using a combination of Z_h and Z_{dr} hydrometeors could be successfully

classified due to their strong discriminating power. Figure 4a seems to show the opposite case, with only Z_{dr} being used, however this is due to the mixing of snow and rain observations creating a far weaker signal. Z_h is poor as a sole classifier when only one scanning elevation is used because high reflectivities could be intense rainfall rather than melting snow. Z_h can still be useful for BB classification on its own, but only when higher or lower elevations are utilised, such as in (Zhang et al 2008; Delrieu et al 2009). LDR shows a good classification performance, however if the freezing levels were higher for the validation events it could perform more poorly due to this measurement suffering from propagation effects (Chandrasekar et al 1994; Bringi and Chandrasekar 2001). LDR greatly aids in determining the full extent of the BB whereas ρ_{hv} had a stronger signal for the inner section of the BB. The signal at the edges could potentially be enhanced through conversion of the ρ_{hv} measurements in to a log scale similarly to LDR, as in Bringi and Chandrasekar (2001). A combination of LDR and ρ_{hv} measurements (Figure 4d) is beneficial for robustness of the algorithm.

3.1. Convective and Stratiform Segregation

Before a correction method is applied, convective and stratiform regions should be segregated and convective rain cells should be classified (Zhang et al. 2008; Delrieu et al. 2009; Hazenberg et al. 2013). Steiner et al. (1995) present an algorithm with three criteria, in which any pixel with a reflectivity greater than 40 dBZ is classified as convective, and any pixel that is greater by a variable quantity than an average of the surroundings is also classed as convective. In addition, any pixel within a small area surrounding these classified pixels is then determined to be convective. Delrieu et al. (2009) find that the first criteria was too low leading to spurious misidentification, and that the final criteria exacerbated this error. In order to test this classification scheme the initial reflectivity cut-off has been raised to 43 dBZ, as in Delrieu et al. (2009), and the final criteria has been removed. Figure 7 shows the results of the classification during a mixed stratiform, BB, and convective event. The Steiner et al (1995) algorithm can be seen to classify some of the BB as convective precipitation, as it seems to be best applied to error-corrected scans, which was also found to occur by Zhang et al. (2008) and Delrieu et al. (2009). Smyth and Illingworth (1998), and Zhang et al. (2008) use temperature soundings to aid in the precipitation type segregation, however this work aims to only use radar scan data, so a different form will be used.

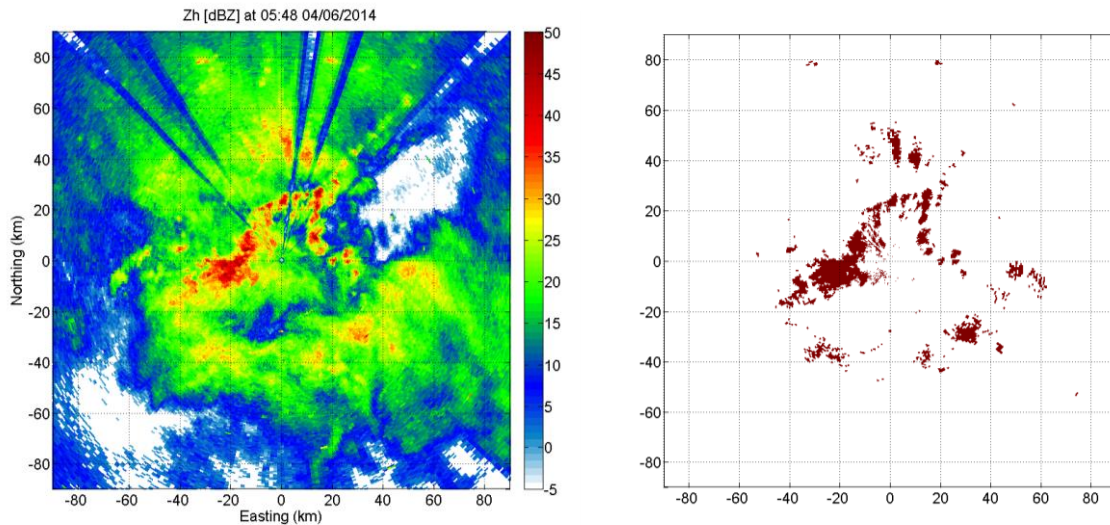


FIG. 5. Output of the Steiner et al (1995) algorithm to classify convective regions, shown in red in (b), with the corresponding radar reflectivity scan in (a).

The output from the melting snow classification algorithm, described previously, can be utilised. The BB correction scheme will only be applied if a consistent BB region of more than 45° in azimuth is observed. Figure 8 shows three different types of unusual events, with a half of a distinct BB (Figure 8a, 8b), a convective situation (Figure 8c, 8d), and a mixed convective and stratiform event (Figure 8e, 8f). The first event does not initially appear to be a BB, however after using the polarimetric measurements the melting snow band appears, and only this region would then be corrected. The second event contains separated rain clouds with intense reflectivity cores, and there is some sparse classification of melting snow, with a larger region of melting snow 75km to the south of the radar. This section would not be corrected for using this algorithm. The third event shows a convective front in the centre of the radar scan which is not classified as melting snow, however the surrounding region has been classified, and as such the correction algorithm would be applied.

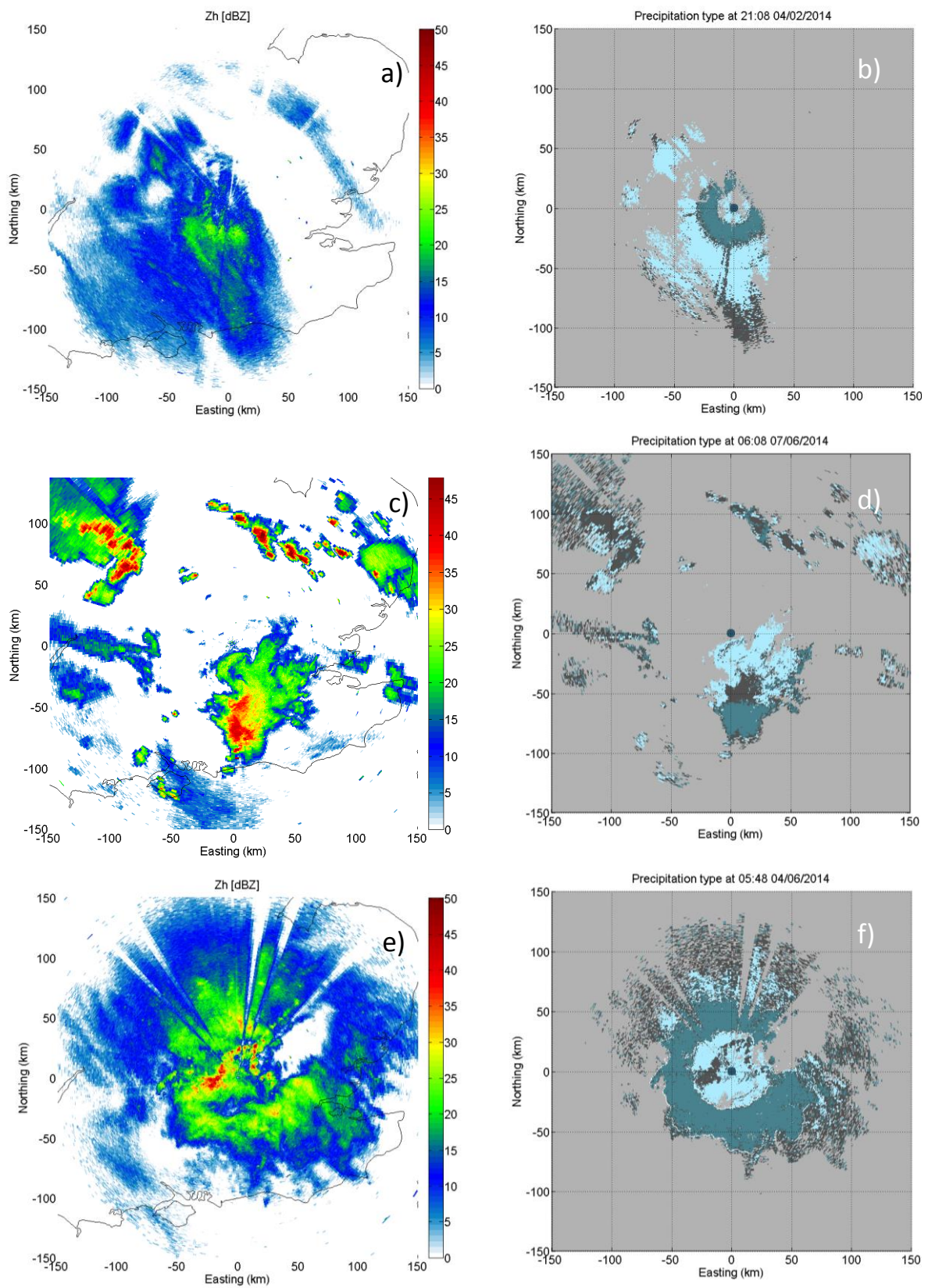


FIG. 6. Three events with different atmospheric conditions. Part (a) shows a stratiform rain band that only partially covers the radar scan, part (c) shows a convective region, and part (e) shows a mixed convective and stratiform rain event. The hydrometeor classification outputs are in parts (b), (d), and (f) for the corresponding radar scans, with dark blue representing melting snow (BB), light blue as rain or snow, and dark grey as unclassified.

3.2 Freezing Level Identification using a Numerical Weather Model

This paper attempts to replicate the BB correction method used operationally by the Met Office in the UK as this will be the benchmark from which to compare to the hydrometeor classification method. The current Met Office operational algorithm identifies the freezing level from Met Office Unified Mesoscale Model forecasts. Data outputs from this model were not available so the 5th generation National Centre for Atmospheric Research (NCAR) mesoscale model (MM5) has been operated instead. This model is widely used and described in (*Grell et al 1994*). Boundary conditions to run the model are from the European Centre for Medium Range Weather

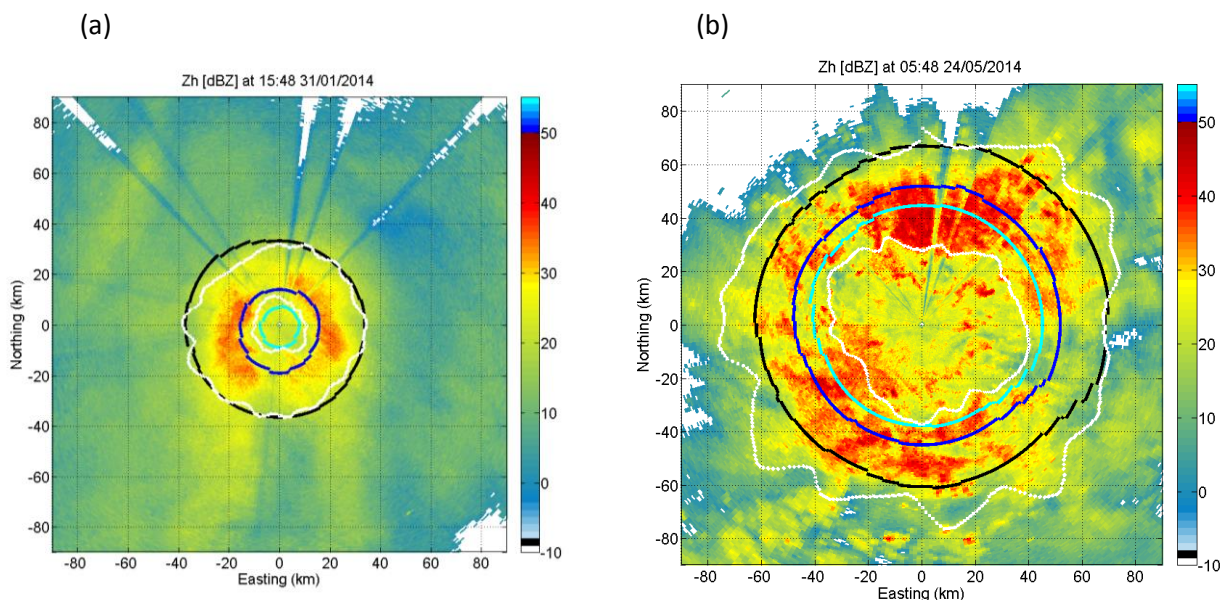


FIG. 7. Comparison of BB classification techniques, with hydrometeor classification (white), MM5 freezing level (black) and BB thicknesses of 500 m (dark blue) and 700 m (light blue) for two events.

Forecasting (ECMWF) ERA-Interim data set. This contains reanalysis data at 1° resolution. Downscaled reanalysis data should output freezing levels to a higher accuracy in comparison to Numerical Weather Prediction forecasts, so this should counter the effect of using an older NWP model. Freezing level heights are output from the MM5 model over approximately a 300 km region surrounding the Chenies radar with a 6 km resolution and 40 pressure levels. The time step of the model outputs is 1 hour and with over 12 hours allowed either side of the event time for the model to spin up and slow down. The freezing level heights output are converted into polar coordinates to compare to the radar scans, instead of assuming homogeneity as in *Kitchen (1997)*. The BB thickness was suggested to be 500 m from the method described in *Kitchen (1997)* and *Kitchen et al (1994)* suggest a thickness of 700 m. The two thicknesses are compared in Figure 7a in which it can be seen that the 500 m suggestion cuts out the inner portion of the BB whereas the 700 m thickness encloses the whole of the BB area. The MM5 freezing level output compares well with the freezing level from the hydrometeor classification in both images, though the output does not capture the azimuthal variation in the BB thickness, as can be seen in Figure 7b. Figure 8 shows the variation in mean and standard deviation of the BB thickness output by hydrometeor classification through the 7 validation events. The mean thickness reaches 1200 m during an event in May in which there is considerable variation as shown by the large standard deviation. *Zhang et al (2008)* show similar BB thicknesses with monthly mean thicknesses of 820 m for a latitude of 45-50N.

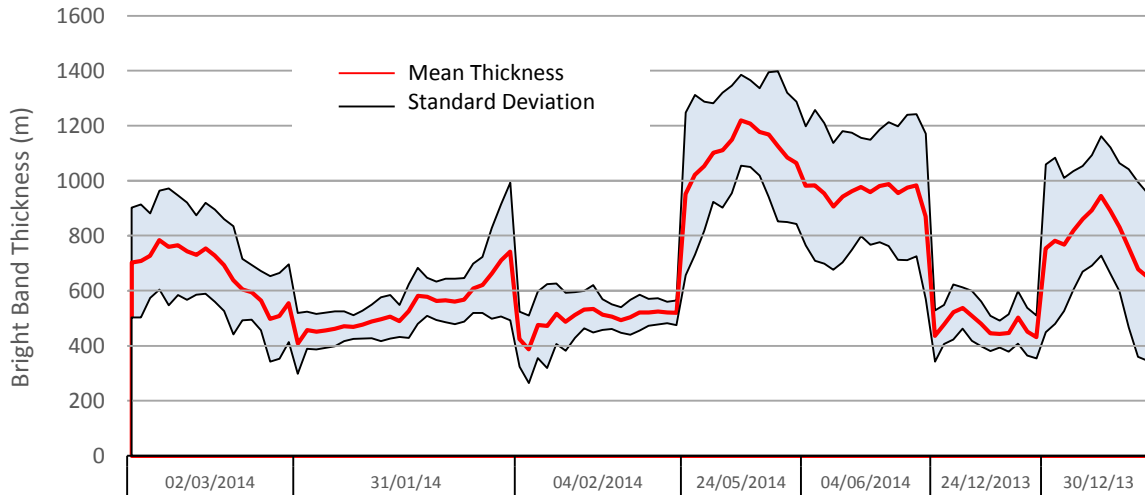


FIG. 8. The mean BB thickness in metres (red central line) output by hydrometeor classification, with standard deviation as the upper and lower bands.

4. Bright Band Correction Schemes

Five different BB classification and correction schemes are implemented and outlined in Figure 9. Three use hydrometeor classification to identify the BB region before applying idealised profiles for correction (HCRR and HCMO) or a mean profile for correction (HCMean). HCRR relies on an idealised VPR defined in *Rico-Ramirez et al (2005)*, and explained further in the following section. HCMO relies on an idealised VPR proposed by *Kitchen et al (1994)* and implemented in the Met Office BB correction scheme. The final two schemes (UKMOMean and UKMO₇₀₀) use freezing level heights output from the MM5 model using reanalysis data. The *Kitchen et al (1994)* idealised VPR is then used for correction for UKMO₇₀₀ with the fixed BB thickness set as 700 m. UKMOMean uses the same mean profile correction scheme as HCMean. In addition to rain gauge comparison, the performance of the VPR corrections will be tested by comparing the corrected scan to an unaltered lower scan. The lower scan will be affected by BB contamination at a further range from the radar and so should display similar reflectivity values at the same range.

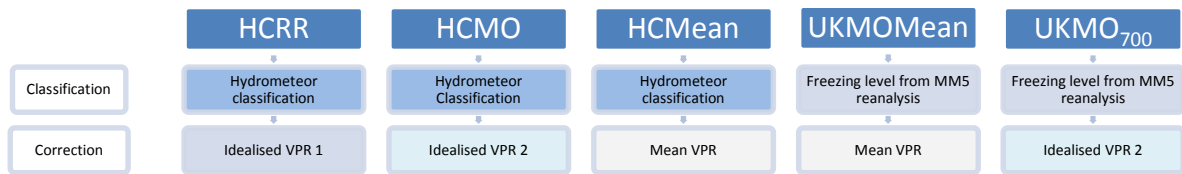


FIG. 9. Outline of the five algorithms, including the two classification techniques described in section 3, and the correction techniques utilising the different VPR formats.

4.1. Idealised VPRs

Idealised VPR 1 (ID1), shown in Figure 10a, is based on extensive experiments conducted using S-band radar at Chilbolton by *Rico-Ramirez et al (2005)*. A database of observed VPRs from Range-Height Indicator (RHI) scans, from which the following equations are formed,

$$\text{ID1:} \quad Z_{peak} = 11.74 + 0.91 * Z_{rain} \quad [\text{in dBZ}] \quad (4)$$

$$Z_{top} = 2.23 + 0.69 * Z_{rain} \quad [\text{in dBZ}] \quad (5)$$

where Z_{rain} is a value of reflectivity in rain expected below the BB that changes iteratively between 10 and 50 dBZ. Z_{top} is the reflectivity at the BB top; above this the reflectivity decreases linearly at a rate of 5 dBZ km⁻¹

with increasing height. Idealised VPR 2 (ID2), shown in Figure 10b, based on *Kitchen* (1997) uses a different equation to form the triangular shaped BB area,

$$\text{ID2:} \quad Z_{\text{peak}} = Z_{\text{rain}} + \frac{252 * Z_{\text{rain}}^{1.42}}{\Delta h_{\text{bb}}} \quad [\text{in mm}^6\text{m}^{-3}] \quad (6)$$

where Δh_{bb} is the BB thickness (mm) and Z_{rain} is in units of mm^6m^{-3} . Above the BB top *Kitchen* (1997) uses two decay constants to describe the exponential decrease in reflectivity. The focus of this paper is not on resolving VPR variations above the BB, so for simplicity the equation for the decay of reflectivity is shown by

$$\text{ID2:} \quad Z(h) = Z_{f_l} * e^{a(h-h_{f_l})} \quad [\text{in mm}^6\text{m}^{-3}] \quad (7)$$

where a is the decay constant, Z_{f_l} is the reflectivity at the freezing level, and h represents the height in the VPR above the freezing level height (h_{f_l}).

Figure 10 displays the two simple idealised profiles in which Z_{peak} is centralised between the BB top and bottom. Idealised profiles have also been tested in which Z_{peak} is matched to the maximum of Z_h within the BB area. In Figure 10a, the Z_{top} value at the BB top is not equal to Z_{rain} below which differs from techniques used by *Fabry and Zawadzki* (1995) and *Kitchen et al* (1994), as in Figure 10b.

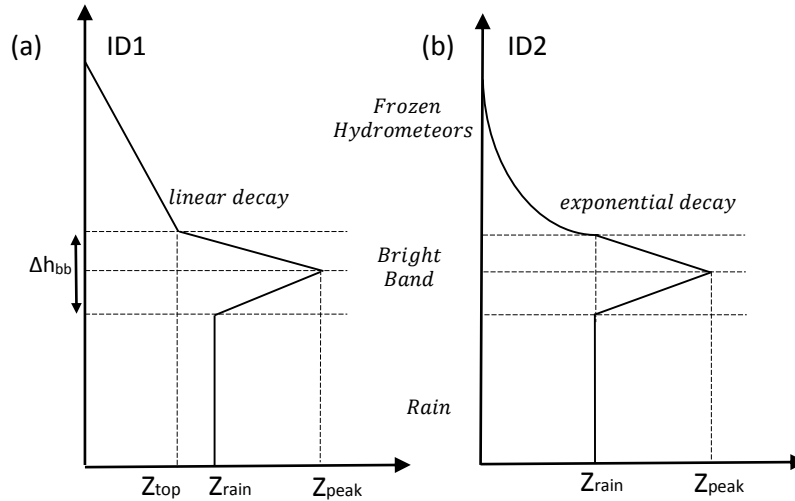


FIG. 10. ID1 (a) and ID2 (b) through stratiform precipitation with the bright band indicated by the lateral dashed lines.

The parameterised VPRs cannot be compared directly to radar values due to the nature of the radar beam. The width of the beam increases with distance so the beam could intersect part of the bright band and the snow above yet only have one value of reflectivity. To resolve this a method proposed by *Brown et al* (1991) and applied by *Kitchen et al* (1994) can be utilised in which the VPR is averaged through the upper and lower limits of the radar beam using the following equations,

$$Z_{\text{ave}} = \int_{\alpha}^{\beta} Z(\theta) f(\theta) d\theta \quad [\text{dBZ}] \quad (8)$$

where $Z(\theta)$ is the modelled VPR value at the angle θ within the beam, α and β represent respectively the bottom and top elevation of the radar beamwidth and $f(\theta)d\theta$ is the fractional beam power at angle θ , as shown in,

$$f(\theta)d\theta = \frac{P(\theta)d\theta}{\int_{\alpha}^{\beta} P(\theta)d\theta} \quad (9)$$

where $P(\theta)$ is the beam power profile, as shown in equation 10, in which k is a constant that will vary according to the beamwidth.

$$P(\theta) = \left[\frac{\sin(k\theta)}{k\theta} \right]^4 \quad (10)$$

For each of the three methods, the idealised profile, after correction based on beam characteristics, is compared to the observed Z_h at every pixel and replaced by the corresponding Z_{rain} value.

4.2 Mean VPR method

The mean VPR method utilises long pulse scanning elevations at 1.4° and 3.0° , and short pulse at 0.9° , 2.0° , 4.0° , 6.0° , and 9.0° . The lowest beam at 0.5° has been ignored as even after clutter has been removed it was found that inclusion of this elevation lead to a poorer performance. The region of data chosen to form the average VPR includes a total of 252,000 points from 7 scanning elevations. The points are averaged azimuthally using a similar method to *Zhang et al* (2008) and *Joss and Lee* (1995), with all reflectivities in the log (dBZ) units. The maximum range of 70 km was chosen after comparing error reduction capabilities with other ranges. *Andrieu and Creutin* (1995) suggest not exceeding 40-50 km, though their results also show that if using a radar with 1° beam width and 1.4° scanning angle this range should be extended. This range needs to have limited variability in precipitation for the average VPR to be representational.

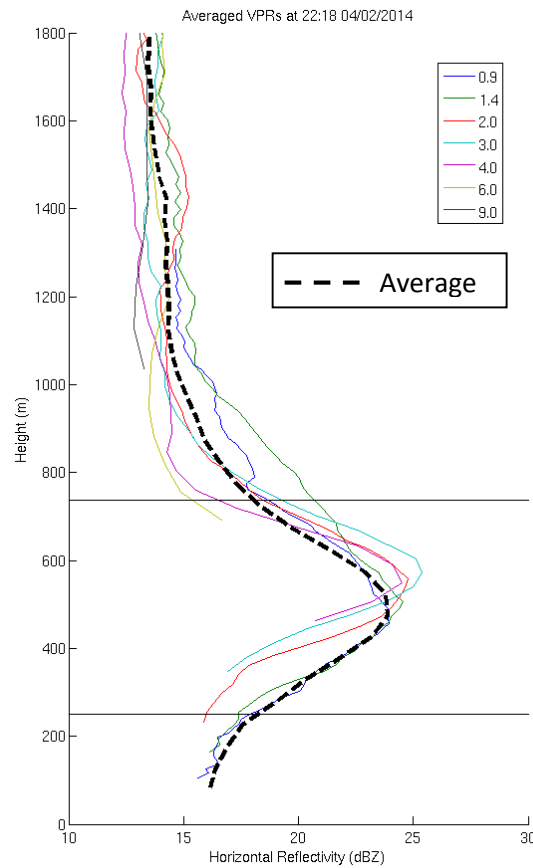


FIG. 11. Averaged VPRs for several elevations (coloured lines), and the total mean profile in dashed black.

The 7 elevation scans are averaged azimuthally to form multiple profiles. These are then split into multiple height bands with 75 m thicknesses and points within the individual bands are averaged over the 60 km range to form one averaged VPR, as shown in Figure 11. A band thickness of 75 m was chosen after experimentation with different numbers. Larger bands with up to 200m thickness, as used in *Zhang et al* (2008), resulted in a far poorer ability to reduce error, whereas 50m and below introduced large variability because too few points were averaged per band. Interpolation between bands further increased the ability of the mean VPR to reduce error.

For quality control purposes reflectivity values below 10 dBZ are excluded and similarly to *Zhang et al* (2008) there must be a minimum of 10 data points when averaging. Once averaged, the profile is normalised with respect to the minimum reflectivity below the BB peak. When there are high reflectivity values below the BB, usually due to convection, normalisation is made difficult due to the small difference between Z_h at the BB peak and Z_h below. The value of Z_h at the top of the BB can be used to counter this. Once the normalised mean VPR is formed it is applied azimuthally, rather than pixel by pixel, in the BB area. The BB top and bottom, identified by hydrometeor classification, are shown by the two horizontal lines in Figure 11.

Beam spreading at longer ranges will cause a reduction in the averaged VPR quality, which is a problem not encountered by the idealised profiles. *Vignal et al* (1999) show how the VPR quality remains high at ranges of 30km but is significantly affected by smoothing at ranges beyond 90km resulting in a less distinct BB curve. At further ranges there will also be discretisation of the profiles due to a decreased number of beams close enough to the ground to capture the precipitation and BB effect (*Andrieu and Creutin* 1995).

5. Results

The corrected reflectivity scans are converted into rain rate through the *Marshall and Palmer* (1948) Z-R equation ($Z = 200 R^{1.6}$), which is widely used for stratiform rain in the UK (*Harrison et al* 2000). The rain rates at a single elevation of 1.4° are then accumulated hourly in order to compare to the hourly co-located rain gauge measurements. Figure 12 shows a scatter plot of initial and corrected radar rainfall estimations, using the HCMO method, against surface based gauge rainfall measurements. The large overestimations by the radar are reduced to be in line with the gauge measurements, however initial underestimations by the radar lead to an increased error. These errors are in part due to the inherent inaccuracies when comparing radar and rain gauge measurements. It can be difficult to quantify these errors without a dense network of gauges, such as in *Villarini and Krajewski* (2008), but this would be beyond the scope of this paper. However, attempts have still been made to reduce the comparison errors by only using gauges that fall within 90 km of the radar. Beyond this the beam thickness reaches nearly 2 km which can lead to underestimations as a part of the beam may be above the hydrometeors. Beyond 90 km from the radar the original MAE is 1.06 mm and the corrected is 0.87 mm, however, within 90 km the original and corrected MAEs are 0.80 and 0.59 mm.

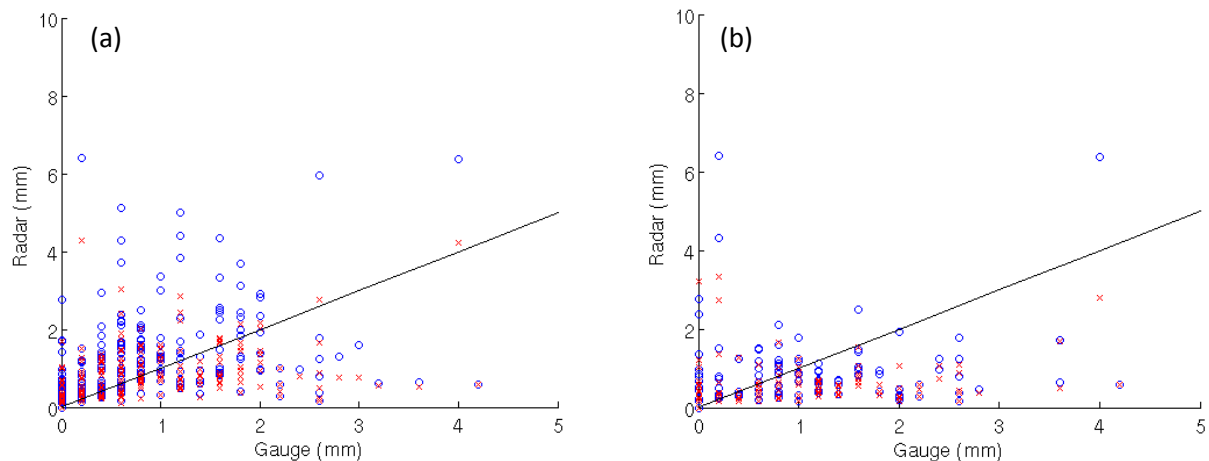


FIG. 12. Scatter plot of rainfall estimated by radar before correction (blue circles) and after correction (red cross) against gauge observations within 90km (a) and beyond 90km (b). Radar scans corrected using the HCK method.

Figure 13 displays the variation in RMSE between radar estimations and gauge observations over the course of the validation events. At 23:00 on 04/02/14 the UKMO₇₀₀ method over corrected the rainfall amounts due to the smaller BB thickness. This method performed well in general, but showed a larger variation, with poor corrections when the BB mean thickness exceeded 700 m. HCRR and HCMO performed consistently well, with HCMean showing a greater variation, sometimes resulting in poorer error reductions than the UKMO₇₀₀ algorithm. Table 1 shows the total errors over all measurement pairs for all samples in addition to points in which the radar initially overestimated the rainfall in comparison to the rain gauge. The hydrometeor classification methods show large improvements; HCMO, which utilises the *Kitchen* (1997) idealised VPR, decreasing the RMSE by 64% and RMB by 91% when there was an initial over estimation. Similarly to *Vignal et al* (2000) the idealised profiles allowed the greatest error reductions. The UKMO₇₀₀ method shows a good error reduction in MAE by 49% and

an especially good RMB reduction. It should be noted however that there is a small sample size with only 142 total rain gauge to radar observation pairs available within the BB areas over the 7 events. The positive bias in the original data, before correction, shows the effect of the BB with increased estimations of rainfall. Looking at all of the data each algorithm then over corrects to obtain a negative bias, but this is likely due to initial underestimation by the radar.

TABLE 1. Statistics for radar to gauge comparisons for uncorrected scans and the correction algorithms. There are 142 total samples and 104 samples in which the radar initially overestimated.

	Algorithm	MAE (mm)	RMSE (mm)	RMB (mm)
All data	Original	0.89	1.34	0.29
	HCRR	0.63	0.90	-0.19
	HCMO	0.61	0.86	-0.24
	HCMean	0.66	0.95	-0.09
	UKMOMean	0.72	1.08	-0.03
	UKMO ₇₀₀	0.66	1.03	-0.19
Initial Over-estimations	Original	1.03	1.57	1.31
	HCRR	0.45	0.70	0.27
	HCMO	0.40	0.56	0.19
	HCMean	0.53	0.83	0.47
	UKMOMean	0.63	1.10	0.60
	UKMO ₇₀₀	0.51	1.00	0.22

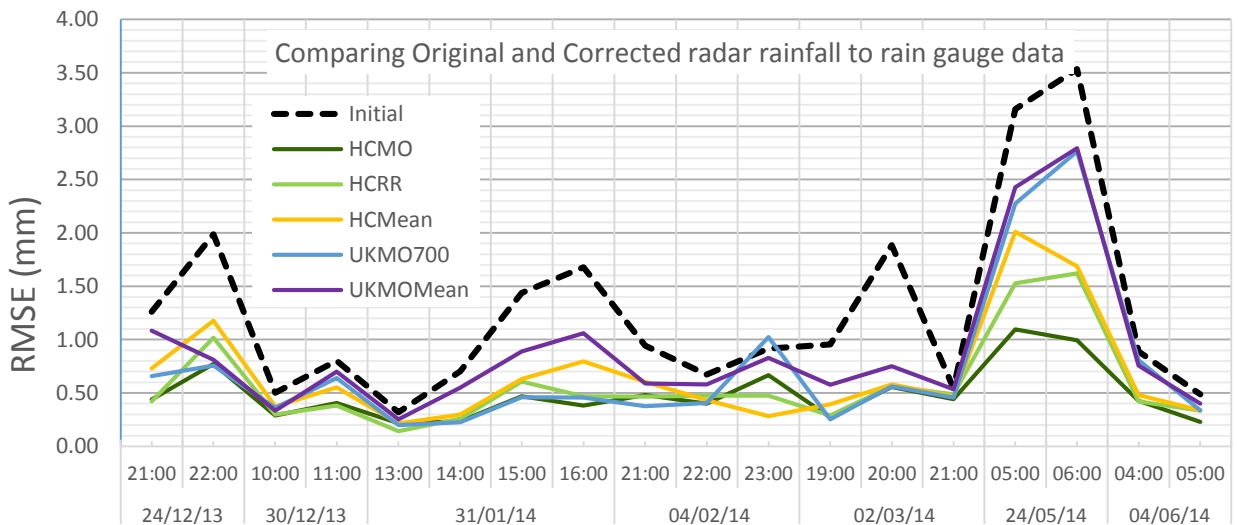


FIG. 13. The RMSE values for uncorrected radar estimates (black dashed) and corrected (coloured) against rain gauge measurements.

In order to increase the number of comparison samples to measure performance, the BB corrected values can be compared to lower elevation scans that are unaffected by the BB at the same range. This will also avoid the errors associated with the Z-R equation and gauge sampling errors. The reflectivities are transformed into rain-rates with the Marshall-Palmer equation to allow a better comparison with the previous results. This transformation will not affect the results as both scans will be converted with the same equation. Table 2 shows the error statistics when corrected scans are compared to lower scans. There is a much larger sample and the two hydrometeor classification methods with idealised profiles (HCRR and HCMO) show large improvements, with HCRR reducing the MAE by 70% compared to 60% by UKMO₇₀₀. Figure 14 shows a similar error distribution

along the events compared to Figure 13, indicating that the events with large errors are not due to larger rain gauge inaccuracies.

TABLE 2. Statistics for comparisons between 1.4° and 0.5° scans for the correction algorithms. There are over 180,000 pixel pairs that are compared.

Algorithm	MAE	RMSE
Original	1.26	2.00
HERR	0.38	0.73
HCMO	0.39	0.77
HCMean	0.51	0.99
UKMOMean	0.76	1.30
UKMO ₇₀₀	0.50	1.00

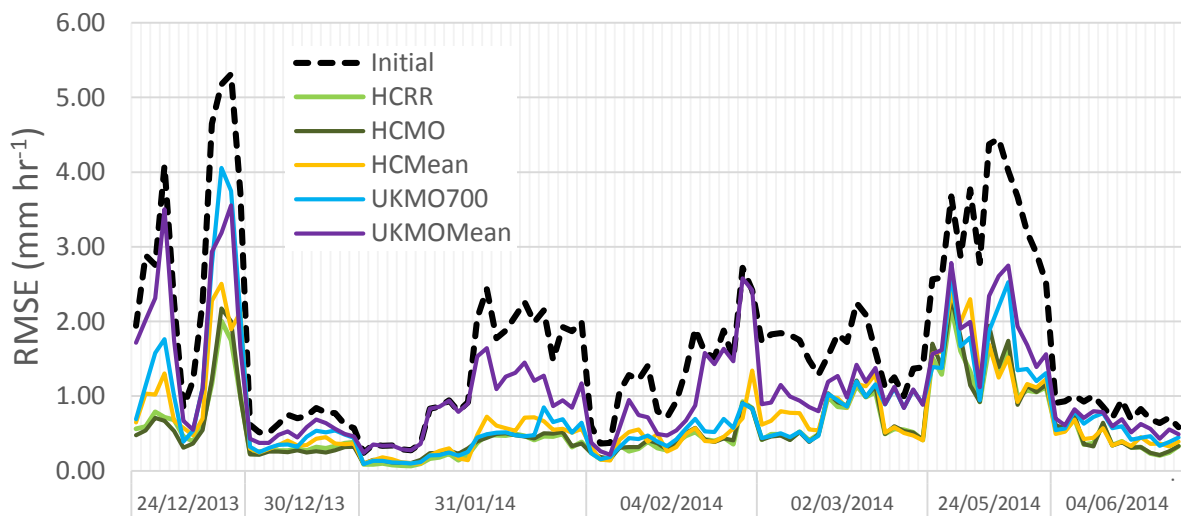


FIG. 14. The RMSE values for uncorrected radar rain rates (black dashed) and corrected (coloured) against lower level scan measurements.

6. Conclusions

Multiple methods were formed for the classification and correction of the BB effect. An algorithm similar to the current UK Met Office method was produced. This involved the input of ECMWF reanalysis data to the MM5 to output freezing level heights along with an assumption of constant BB thickness. Due to the recent adoption of operational dual-polarimetric radars in the UK a real time algorithm was formed as an alternative method for classification of the BB region. A fuzzy logic system was used with a large database of input vales to classify melting snow. The ability of two idealised profiles are compared to a mean profile for BB correction.

The correction schemes were tested through comparison of the corrected radar rainfall estimations against surface rain gauge measurements and lower level uncorrected scans. A total of 14 events were used for the project, 7 of which were used in validation. Following the Met Office method the RMSE was reduced by a factor of 2 in comparison to lower scans. When using the same idealised profile for correction the hydrometeor classification method for BB identification reduced the error by a further 11%. Hydrometeor classification makes an allowance for variation in the size and shape of the BB area, whereas the freezing level forecast method relies on a constant thickness. The main benefit of hydrometeor classification is that it relies only on measurements from the radar itself, rather than inputs from computationally intensive model runs.

Acknowledgements

The authors would like to thank the UK Met Office for providing the polarimetric radar data and MIDAS rain gauge sets through the British Atmospheric Data Centre, in addition to the Environment Agency for their gauge data.

References

- Andrieu H., and J.D. Creutin, 1995: Identification of vertical profiles of radar reflectivity for hydrological applications using an inverse method. Part I: Formulation. *J. Appl. Meteor.*, **34**, 225–239.
- Atlas D., and H.C. Banks, 1950: A virtual echo-layer above the bright band. *J. Atmos. Sci.*, **7**, 402–403.
- Austin P.M., and A.C. Bemis, 1950: A quantitative study of the bright band in radar precipitation echoes. *J. Meteor.*, **7**, 145–151.
- Aydin K., Y. Zhao, and T.A. Seliga, 1990: A Differential Reflectivity Radar Hall Measurement Technique: Observations during the Denver Hailstorm of 13 June 1984. *J. Atmos. Oceanic Technol.*, **7**, 104–113.
- Brandes E.A., and K. Ikeda, 2004: Freezing-level estimation with polarimetric radar. *J. Appl. Meteor.*, **43**:11, 1541–1553.
- Bringi V.N., and V. Chandreskar, 2001: Polarimetric Doppler weather radar, principles and applications. Cambridge University Press, New York, 636pp.
- Brown R., G.P. Sargent, and R.M. Blackall, 1991: Range and orographic corrections for use in real-time radar data analysis. *Hydrological applications of weather radar*, 219–228.
- Caylor I.J., et al, 1990: Bright band errors in radar estimates of rainfall: Identification and correction using polarization diversity. 294–303, in *Weather Radar Networking*, (edited by C.G. Collier & M. Chapuis), COST Project 73, EUR 12414 EN-FR. Document EUCO-COST 73/52/90.
- Ciach G.J., 2003: Local Random Errors in Tipping-Bucket Rain Gauge Measurements. *J. Atmos. Oceanic Technol.*, **20**, 752–759.
- Delrieu G., et al, 2009: Bollène-2002 Experiment: Radar Quantitative Precipitation Estimation in the Cévennes–Vivarais Region, France. *J. Appl. Meteor. Climatol.*, **48**, 1422–1447.
- Fabry F., and I. Zawadzki, 1995: Long-Term Radar Observations of the Melting Layer of Precipitation and Their Interpretation. *J. Atmos. Sci.*, **52**, 838–851.
- Grell, G., J. Dudhia, and D. Stauffer, 1994: A description of the fifth generation Penn State/NCAR Mesoscale Model (MM5). NCAR Tech. Note NCAR/TN-398 1 STR, 117 pp.
- Habib E., W. Krajewski, and A. Kruger, 2001: Sampling Errors of Tipping-Bucket Rain Gauge Measurements. *J. Hydrol. Eng.*, **6**:2, 159–166.
- Hall W., M.A. Rico-Ramirez, and K. Stefan, 2014: Classification and correction of the radar bright band with polarimetric radar, in: 8th European Conference on Radar in Meteorology and Hydrology, Garmisch-Partenkirchen, Germany.
- Harrison D.L., S.J. Driscoll, and M. Kitchen, 2000: Improving precipitation estimates from weather radar using quality control and correction techniques, *Met Apps*, **7**:02, 135–144.
- Hazenbergh, P., et al, 2013: Identification and uncertainty estimation of vertical reflectivity profiles using a Lagrangian approach to support quantitative precipitation measurements by weather radar. *J. Geophys. Res. Atmos.*, **118**, 10,243–10,261.
- Herzogh P.H., and A.R. Jameson, 1992: Observing precipitation through dual-polarisation radar measurements. *Bull. Amer. Meteor. Soc.* **73**, 1365–1374.
- Illingworth A., and R. Thompson, 2012: Radar bright band correction using linear depolarisation ratio. In: International Symposium on Weather Radar and Hydrology (WRaH 2011), 18–21 Apr 2011, Exeter, UK, pp. 64–68.
- Joss J., and A. Waldvogel, 1990: Precipitation measurement and hydrology. In *Radar in Meteorology: Battan Memorial and 40th Anniversary Radar Meteorology Conference*, Atlas D (ed). American Meteorological Society: Boston, MA; 577–606.
- Kirstetter P., et al, 2013: A Physically Based Identification of Vertical Profiles of Reflectivity from Volume Scan Radar Data. *J. Appl. Meteor. Climatol.*, **52**(7), 1645–1663.
- Kitchen M., R. Brown, and A.G. Davies, 1994: Real time correction of weather radar data for the effects of bright band, range and orographic growth in widespread precipitation. *Q. J. R. Meteor. Soc.* **120**, 1231–1254.
- , 1997: Toward improved radar estimates of surface precipitation at long range. *Q.J.R. Meteor. Soc.*, **120**, 145–163.
- Koistinen J. 1991: Operational correction of radar rainfall errors due to the vertical reflectivity profile. Preprints, 25th Int. Conf. on Radar Meteorology, Vol. 1, Paris, France, Amer. Meteor. Soc., 91–94.
- Liu H., and V. Chandrasekar, 2000: Classification of Hydrometeors Based on Polarimetric Radar Measurements: Development of Fuzzy Logic and Neuro-Fuzzy Systems, and In Situ Verification. *J. Atmos. Oceanic Technol.*, **17**, 140–164.
- Marshall J. and W. Palmer, 1948: The distribution of raindrops with size. *J. Meteor.*, **5**, 165–166.
- Matrosov S.Y., K.A. Clark, and D.E. Kingsmill, 2007: A Polarimetric Radar Approach to Identify Rain, Melting-Layer, and Snow Regions for Applying Corrections to Vertical Profiles of Reflectivity. *J. Appl. Meteor. Climatol.*, **46**, 154–166.
- Mendel J.M., 1995: Fuzzy logic systems for engineering: a tutorial. *Proceedings of the IEEE*, **83**(3), 345–377.
- Park H.S., et al, 2009: The Hydrometeor Classification Algorithm for the Polarimetric WSR-88D: Description and Application to an MCS. *Wea. Forecasting*, **24**, 730–748.
- Qi Y., J. Zhang, and P. Zhang, 2013: A real-time automated convective and stratiform precipitation segregation algorithm in native radar coordinates, *Q.J.R. Meteor. Soc.*, **139**(677), 2233–2240.
- Rico-Ramirez M.A., I.D. Cluckie, and D. Han, 2005: Correction of the bright band using dual-polarisation radar. *Atmos. Sci. Lett.*, **6**, 40–46.
- and I.D. Cluckie, 2008: Classification of Ground Clutter and Anomalous Propagation Using Dual-Polarization Weather Radar, *IEEE Trans. Geosci. Remote Sens.*, **46**(7), 1892–1904.
- Ryzhkov A. and D. Zrnich, 1998: Discrimination between Rain and Snow with a Polarimetric Radar. *J. Appl. Meteor.*, **37**, 1228–1240.
- Sanchez-Diezma R., I. Zawadzki, and D. Sempere-Torres, 2000: Identification of the bright band through the analysis of volumetric radar data. *J. Geophys. Res.*, **105**, 2225–2236.

- Shusse, Y., et al, 2011: Polarimetric Radar Observation of the Melting Layer in a Convective Rainfall System during the Rainy Season over the East China Sea. *J. Appl. Meteor. Climatol.*, **50**, 354–367.
- Steiner, M., R.A. Houze Jr., and S.E. Yuter, 1995: Climatological Characterization of Three-Dimensional Storm Structure from Operational Radar and Rain Gauge Data. *J. Appl. Meteor.*, **34**, 1978–2007.
- , et al, 1999: Effect of bias adjustment and rain gauge data quality control on radar rainfall estimation. *Water Resour. Res.*, **35**, 2487–2503.
- Straka J., D. Zrnić, and A. Ryzhkov, 2000: Bulk Hydrometeor Classification and Quantification Using Polarimetric Radar Data: Synthesis of Relations. *J. Appl. Meteor.*, **39**, 1341–1372.
- and D. Zrnić 1993: An algorithm to deduce hydrometeor types and contents from multiparameter radar data. *Preprints, 26th Int. Conf. on Radar Meteorology, Vol. 1, Norman, OK, Amer. Meteor. Soc.*, 513-515.
- Tabary P., et al, 2007: The New French Operational Radar Rainfall Product. Part II: Validation. *Wea. Forecasting*, **22**, 409-427.
- Vignal B. et al, 2000: Three methods to determine profiles of reflectivity from volumetric radar data to correct precipitation estimates. *J. Appl. Meteor.*, **39(10)**, 1715-1726.
- , H. Andrieu, and J.D. Creutin, 1999: Identification of Vertical Profiles of Reflectivity from Volume Scan Radar Data. *J. Appl. Meteor.*, **38**, 1214–1228.
- Villarini G., and W.F. Krajewski, 2010: Review of the different sources of uncertainty in single polarization radar-based estimates of rainfall. *Surv. Geophys.* **31**, 107-129
- Vivekanandan J., et al, 1999: Cloud microphysics retrieval using S-band dual-polarization radar measurements. *Bull. Amer. Meteor. Soc.*, **80**, 381–388.
- Zhang J., C. Langston, and K. Howard, 2008: Brightband Identification Based on Vertical Profiles of Reflectivity from the WSR-88D. *J. Atmos. Oceanic Technol.*, **25**, 1859–1872.
- J., and Y. Qi, 2010: A Real-Time Algorithm for the Correction of Brightband Effects in Radar-Derived QPE. *J. Hydrometeor.*, **11**, 1157–1171.
- Zrnić D., et al, 2001: Testing a Procedure for Automatic Classification of Hydrometeor Types. *J. Atmos. Oceanic Technol.*, **18**, 892–913.